crystals

MDPI

Article

Mesomorphic, Optical and DFT Aspects of Near to Room-Temperature Calamitic Liquid Crystal

Ayman A. Zaki [1,2], Mohamed Hagar [3,4,*], Rua B. Alnoman [3], Mariusz Jaremko [5], Abdul-Hamid Emwas [6] and Hoda A. Ahmed [7,*]

1 Physics Department, College of Sciences, Taibah University, Yanbu 30799, Saudi Arabia; aismail@taibahu.edu.sa
2 Physics Department, Faculty of Sciences, Banha University, Banha 13511, Egypt
3 Chemistry Department, College of Sciences, Taibah University, Yanbu 30799, Saudi Arabia; rua-b-n@live.co.uk
4 Faculty of Science, Chemistry Department, Alexandria University, Alexandria 21321, Egypt
5 Biological and Environmental Sciences & Engineering Division (BESE), King Abdullah University of Science and Technology (KAUST), Thuwal, 23955-6900, Saudi Arabia; Mariusz.jaremko@kaust.edu.sa
6 Core Labs., King Abdullah University of Science and Technology, Thuwal 23955-6900, Saudi Arabia; abdelhamid.emwas@kaust.edu.sa
7 Department of Chemistry, Faculty of Science, Cairo University, Cairo 12613, Egypt
* Correspondence: mhagar@taibahu.edu.sa (M.H.); ahoda@sci.cu.edu.eg (H.A.A.)

Received: 25 September 2020; Accepted: 6 November 2020; Published: 16 November 2020

Abstract: A new liquid crystalline, optical material-based Schiff base core with a near to room-temperature mesophase, (4-methoxybenzylideneamino)phenyl oleate (I), was prepared from a natural fatty acid derivative, and its physical and chemical properties investigated by experimental and theoretical approaches. The molecular structure was confirmed by elemental analysis, FT-IR (Fourier-Transform-Infrared Spectroscopy) and NMR (nuclear magnetic resonance) spectroscopy. Optical and mesomorphic activities were characterized by differential scanning calorimetry (DSC) and polarized optical microscopy (POM). The results show that compound (I) exhibits an enantiotropic monomorphic phase comprising a smectic A phase within the near to room-temperature range. Ordinary and extraordinary refractive indices as well as birefringence with changeable temperatures were analyzed. Microscopic and macroscopic order parameters were also calculated. Theoretical density functional theory (DFT) calculations were carried out to estimate the geometrical molecular structures of the prepared compounds, and the DFT results were used to illustrate the mesomorphic results and optical characteristics in terms of their predicted data. Three geometrical isomers of the prepared compound were investigated to predict the most stable isomer. Many parameters were affected by the geometrical isomerism such as aspect ratio, planarity, and dipole moment. Thermal parameters of the theoretical calculations revealed that the highest co-planar aromatic core is the most stable conformer.

Keywords: near to room-temperature mesophase; optical properties; refractive index; birefringence; geometrical parameters; DFT calculations

1. Introduction

Liquid crystals (LCs) of low melting temperatures are important materials for a wide range of applications, including temperature sensors and electro-optical displays [1–6]. These materials require certain characteristics to be manageable in device applications [1,2,7]. The applicable liquid crystalline compounds depend on various parameters, such as optical transmittance, absorption coefficient,

order parameter, dielectric constant, and birefringence, amongst others. In addition, mesomorphic type and stability also contribute essential characteristics. Color change with temperature is also a valuable phenomenon in the liquid crystals field [8]. Thus, in thermotropic LCs, the transmittance has been investigated in different LC mesophases [9]. Many liquid crystalline derivatives possess one or more distinct phases depending on the molecular order of the mesophase [10–12].

The thermal stability of mesomorphic molecules is mainly affected by the character of the bonds in the molecule, particularly the types of end groups [13–15]. It is also a sensible parameter allowing for the evaluation of the stability of liquid crystalline compounds because heating some chemical species can reveal those that can conduct electric currents [16]. Most investigations have focused on Schiff's bases since the discovery of 4-methoxybenzylidene-4′-butylaniline (MBBA), which possesses a room temperature nematic phase [17].

The refractive index and birefringence measurements can be obtained using an Abbe refractometer and the wedge method, and Newton's ring technique for the N and Sm A phases [11,18–20]. Yildiz et al. [21] measured the ordinary and extraordinary refractive indices of the 4-butyloxyphenyl-4′-decyloxybenzoate ($10O_4$) liquid crystal in the nematic phase. The refractive index dependence of temperature in the isotropic, nematic and smectic A phases were obtained. Moreover, the optical birefringence based on a rotating-analyzer method has been investigated [18,22]. Moreover, the temperature dependence of the ordinary (n_o) and extraordinary (n_e) refractive indices, and birefringence (Δn) for thermotropic LCs mesogens have been reported [23]. Recently, ordinary and extraordinary refractive indices and birefringence at variable temperatures have been estimated for azopyridine-based supramolecular complexes and their individuals, as well as the evaluation of microscopic and macroscopic order parameters [24]. Elsewhere, the orientation effect of two laterally fluorine atoms in difluorophenylazophenyl Benzoate compounds on the refractive indices and birefringence order parameters were investigated using an Abbe refractometer and modified spectrophotometer techniques [25,26].

The molecular structure and its associated geometrical properties could also be helpful tools to design an essential material for an innovative device with superior functions and applications. Several reports show that the deformation of architectures of the molecules can affect the behavior of the mesomorphic compounds [27–29]. In general, the changes of polarity and/or polarizability of the central core can influence the stability of the mesophase of the prepared compound. In comparison with our previously reported fatty acid liquid crystals [2,30], the terminal substituents that are either small polar compact groups or flexible long chains affect the molecular structure of the LC materials [31].

It has been reported that the low molar mass calamitic LCs comprising two aromatic rings and one or more terminal substituent, i.e., 4-methoxybenzylidene-4′-butylaniline, are able to form a nematic phase at room temperature [17,32–34]. Moreover, attachment polar groups between the two isomeric molecules could lead to a further decrease in the melting points of their mixed systems. Thus, for the synthesis of thermotropic LCs for certain applications, we have been focusing on the selection of terminal wings, flexible alkyl/alkoxy chains, and the mesogenic core [2,30,35].

Schiff base linkage offers a stepped core geometry while retaining molecular linearity, thereby providing improved mesomorphic stability and induced mesophase formation [36]. Therefore, it can play an important role as a spacer unit in the depression of melting temperature with a required range of applications. The new design of functional materials with novel architectures is an important area of interest in geometrical approaches [27,37,38]. Our recent studies are focused on the correlation between the mesomorphic transition data and the evaluated computational calculations for synthesized materials.

In order to better understand the structural effect relationship of natural fatty alkenyl terminals, the mesophase characteristics of new groups of azobenzene liquid crystalline derivatives based on naturally occurring fatty acids were reported [2]. In a recent study, the optical isomeric geometrical characterizations of new non-symmetric azomethine natural fatty acid derivatives were investigated [30]. It was found that the mesomorphic properties and geometrical expectations were impacted in a different

way by exchanging the mesogenic core. These findings encouraged us to study the synthesis and analysis of another calamitic molecule with an inverted azomethine linkage core.

Based on the above consideration, and in order to achieve low melting temperatures near to room temperature, a new two-ring calamitic compound with an azomethine central linkage, namely (4-methoxyphenylimino)methyl)phenyl oleate (**I**), was synthesized, and its mesomorphic and optical behaviour investigated using experimental and theoretical approaches. Additionally, the ordinary and extraordinary refractive indices, birefringence, thermal stability and order parameters were measured. The optical activity data were correlated to geometrical results from simulated DFT modeling calculations.

2. Experimental

2.1. Materials

4-methoxyaniline, oleic acid natural fatty acid, and 4-hydroxybenzaldehyde were obtained from Sigma-Aldrich (Hamburg, Germany). *N,N*′-dicyclohexylcarbodiimide (DCC), 4-dimethylaminopyridine (DMAP), dichloromethane ethanol and methanol were purchased from Aldrich (Wisconsin, USA). All chemicals were used without further purification.

2.2. Synthesis of (4-methoxybenzylideneamino)phenyl oleate, I

I was prepared according to the following Scheme 1:

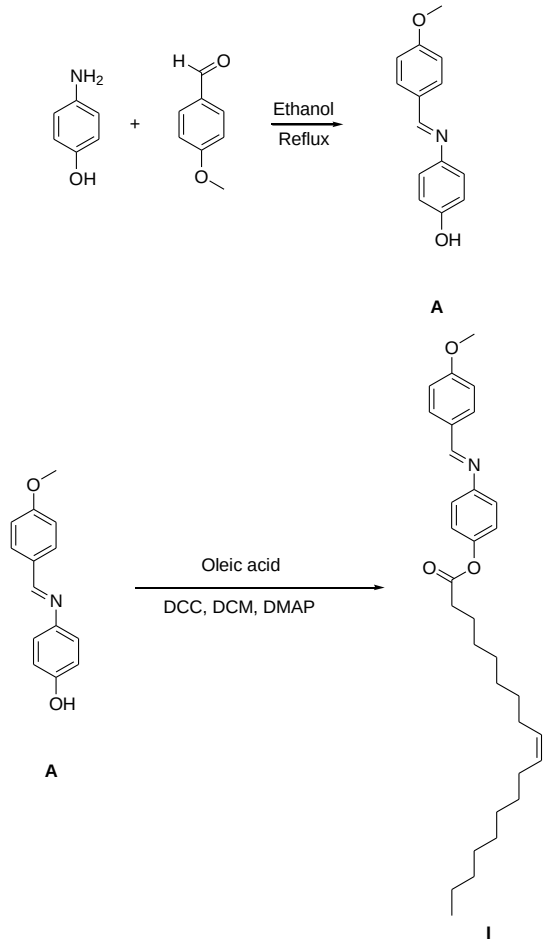

Scheme 1. Synthesis of(4-methoxybenzylideneamino)phenyl oleate, **I**.

2.3. Synthesis

2.3.1. Synthesis of 4-methoxybenzylideneamino)phenol **A**:

Equimolars of 4-methoxybenzaldehyde (4.1 mmol) and 4-aminophenol (4.1 mmol) in ethanol (10 mL) were refluxed for 2 h. The reaction mixture was allowed to cool, and the separated product filtered. The obtained solid was recrystallized from ethanol.

2.3.2. Synthesis of (4-methoxybenzylideneamino)phenyl oleate, I

Equimolar equivalents of (4-methoxybenzylideneamino)phenol **A** (4.1 mmol) and 4-aleic acid (4.1 mmol) were dissolved in 25 mL dry methylene chloride. *N*,*N*′-dicyclohexylcarbodiimide (DCC, 0.02 mole) and a few crystals of 4-dimethylaminopyridine (DMAP) as a catalyst were added. The mixture was left to stand for 72 h at room temperature with continuous stirring. The solid residue obtained was recrystallized twice from ethanol.

Yield = 94.7%, m.p. = 41.9 °C, ^{1}H NMR (600 MHz, DMSO) δ 8.37 (s, 1H CH=N), 7.85 (d, *J* = 8.7 Hz, 2H, Ar-H), 7.20 (d, *J* = 8.6 Hz, 2H, Ar-H), 7.09 (d, *J* = 8.6 Hz, 2H, Ar-H), 6.99 (d, *J* = 8.7 Hz, 2H, Ar-H), 5.98 (m, 1H, CH=), 5.96 (m, 1H, CH=), 3.87 (s, 3H, OCH_3), 2.55 (t, *J* = 7.5 Hz, 2H), 2.11–1.95 (m, 4H), 1.78–1.69 (m, 2H), 1.53–1.07 (m, 22H), 0.87 (t, *J* = 6.9 Hz, 3H, CH_3). ^{13}C NMR (151 MHz, DMSO) δ = 169.24 (C=O), 158.86 (C=N), 156.44 (C-Ar), 146.42 (C-Ar), 145.04 (C-Ar), 127.24 (CH-Ar), 126.76 (CH=), 126.46 (C-Ar), 125.70 (C-Ar), 118.93 (CH-Ar), 118.35 (CH-Ar), 110.91 (CH-Ar), 52.25 (OCH_3), 30.99 (CH_2), 30.56 (CH_2), 28.55 (CH_2), 26.42 (CH_2), 26.34 (CH_2), 26.18 (CH_2), 25.98 (CH_2), 25.81 (CH_2), 25.75 (CH_2), 25.72(CH_2), 23.84(CH_2), 22.27 (CH_2), 21.62 (CH_2), 19.38 (CH_3).

3. Results and Discussion

Nuclear magnetic resonance (NMR) spectroscopy is a versatile analytical tool that has been extensively used in chemistry and in the identification of liquid crystals [39]. The great strength of NMR is the ability to distinguish the unique magnetic environments of the same type of nuclei (e.g., ^{1}H and ^{13}C) in different positions of the same molecule, enabling researchers to investigate molecules at the atomic level. Thus, NMR is a powerful tool to study molecular dynamics, and can be used to elucidate different structures of the same molecule, and to monitor the associated kinetics [40] and thermodynamics of the changes that could be caused by changing sample temperature. Molecular dynamics of the antiferroelectric liquid crystal can be investigated using different nuclear magnetic resonance (NMR) techniques.

The molecular formula of the prepared compound **I** was confirmed via its elemental analysis, FT-IR data and NMR spectroscopy. The results were consistent with the projected structure. The ^{1}H-NMR and ^{13}C-NMR for the methoxy group appeared at δ = 3.87 and 52.25 ppm, respectively. However, the alkenyl protons appeared at δ = 5.96 and 5.89 ppm as two multiplets. The signal 8.60 was assigned to the CH=N proton, and the corresponding carbon appeared at 158.8 ppm. The NMR peaks between 7–7.4 ppm were assigned to the ^{1}H aromatic resonances frequencies, while ^{13}C peaks were observed at 158–110 ppm.

Schiff bases as well as azo derivatives are the kind of compounds that can be present in two forms, *E* and *Z* isomers, but these compounds present only in the *E* form in the solid state [41,42]. The *Z* form could be obtained either by UV irradiation or thermal heating. In this study, the NMR spectra were recorded at different temperatures to investigate the molecular dynamics and to probe any conformational or structural changes in response to temperature variations (Supplementary Material). The NMR was recorded at different temperatures (see Figure S1) and the chemical shifts associated with each signal are presented in Table S1. The results of the NMR at various temperatures revealed that there is no significant effect on the chemical shifts of the recorded signals, indicating that compound **I** is thermally stable. As shown in Figure 1, the thermal heating at 365 K of the DMSO solution of the prepared compound resulted in a new peak observed at (δ = 9.9 of the CH=N). These results provide clear evidence of the formation of the *Z* isomer. The percentage of *E* and *Z* isomers is calculated from

the ratio of integral intensities of the CH=N protons of both signals. The ratio between the *Z*:*E* isomers ranged between 1 and 89 at a temperature range of 345–365 K.

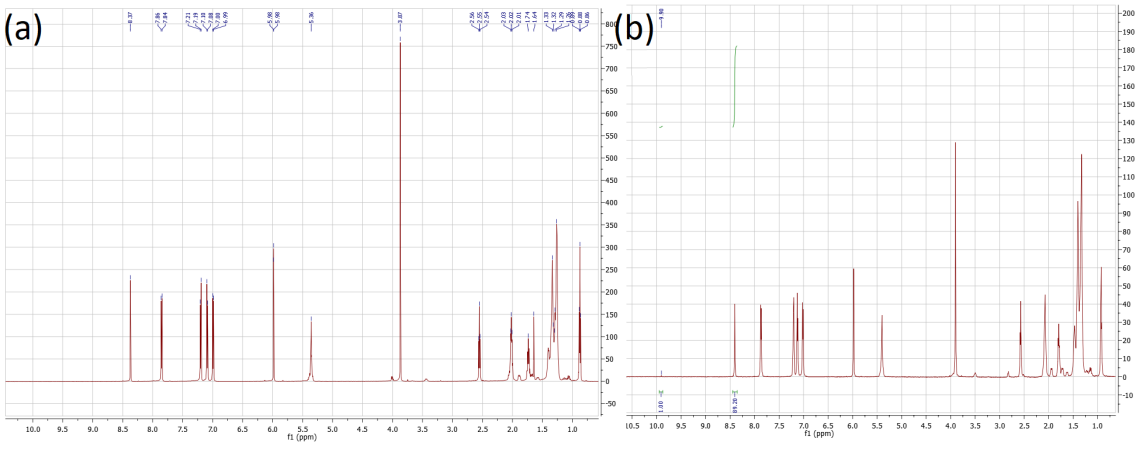

Figure 1. ^{1}H-NMR of (4-methoxybenzylideneamino)phenyl oleate at 305 K (**a**) and 365 K (**b**).

3.1. Mesomorphic Behavior Studies

Mesomorphic and optical activity of the synthesized oleic acid natural fatty acid derivative (**I**) were investigated by differential scanning calorimetry (DSC), and textures were confirmed by polarizing optical microscopy (POM). DSC thermograms of the present compound, **I**, during heating /cooling scans are presented in Figure 2. These showed two endotherm peaks of the crystal–smectic A and smectic A–isotropic transitions during heating and cooling scans. The POM showed a focal conic fan characteristic of the SmA phase (Figure 3). Details of the transition temperatures and enthalpies as well as the normalized entropy of transition, as derived from DSC measurements during heating and cooling scans, are presented in Table 1. In order to ensure the stability of the synthesized compound, DSC measurements were performed for two heating–cooling cycles. Thermal analyses of this derivative (**I**) were recorded from the second heating scan. Moreover, DSC measurements were confirmed by the POM texture observations. Figure 2; Figure 3 indicate that the prepared compound exhibits enantiotropic monomorphic properties and possesses a smectogenic mesophase (SmA phase).

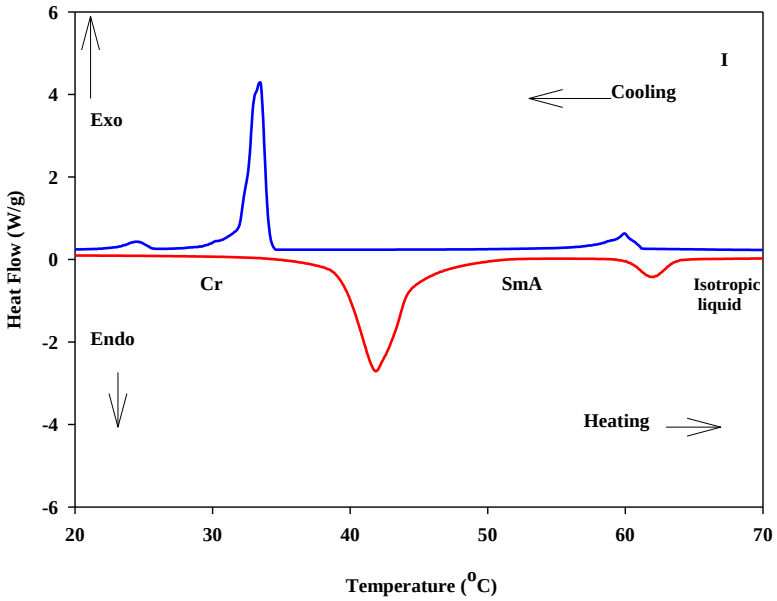

Figure 2. Differential scanning calorimetry (DSC) thermograms upon heating/cooling cycles of compound **I** with heating rate 10 °C/min.

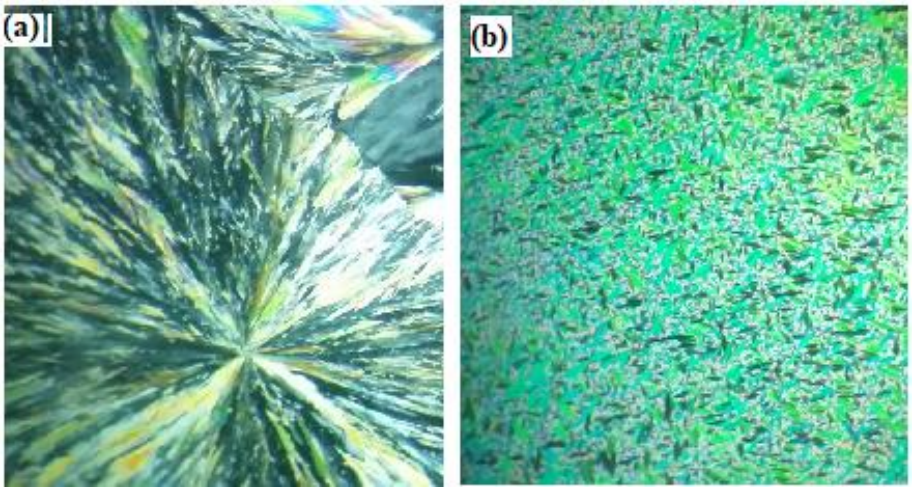

Figure 3. Optical photomicrographs under polarized optical microscopy (POM) of the compound **I** during the cooling scan. (**a**) Crystal phase at 20 °C and (**b**) SmA phase at 37.0 °C.

Table 1. Phase transition temperatures (°C), enthalpy of transition **ΔH** (kJ/mol), and normalized entropy of transition, **Δ*S*/R** for compound **I** upon heating/cooling cycles.

Heating Process	$T_{\text{Cr-SmA}}$	$\Delta H_{\text{Cr-SmA}}$	$T_{\text{SmA-I}}$	$\Delta H_{\text{SmA-I}}$	$\Delta S_{\text{SmA-I}}/\text{R}$
Cooling Process	41.9	35.78	62	2.98	1.07
	$T_{\text{I-SmA}}$	$\Delta H_{\text{I-SmA}}$	$T_{\text{SmA-Cr}}$	$\Delta H_{\text{SmA-Cr}}$	$\Delta S_{\text{I-SmA}}/\text{R}$
	60	2.41	33.5	31.9	0.87

Cr-I = transition from solid to isotropic phase. Cr-SmA = transition from solid to SmA phase. SmA-I = transition from SmA to isotropic phase. I-SmA = transition from solid to SmA phase. SmA-Cr = transition from SmA to solid phase. **Δ*S*/R** = normalized entropy of transition.

As shown from Table 1 and Figure 2; Figure 3, the oleic acid derivative (**I**) produces a mesomorphic compound with low melting temperature near room temperature (41.9 °C upon heating) that was augmented by the long length of the saturated alkenyl terminal chain. The terminal interactions participate in an important role in the determination of the SmA-to-isotropic behavior, i.e., the enhancement of the smectic molecular order is set by the fact that the terminal attractions become stronger, permitting the simple arrangement of the layers due to the long alkenyl chain, enhancing the SmA-to-I transition. Furthermore, the smectic phase formation may be due to the microphase separation between the alkenyl chains and aromatic cores, which becomes more favorable as the length of the terminal chain increases [43,44]. Moreover, the mesomorphic range of compound **I** is ≈ 20 °C upon heating and ≈ 26.5 °C on cooling. Generally, the mesomorphic behavior of calamitic mesogens is impacted by many parameters, such as the dipole moment, aspect ratio, polarizability and the competitive interaction between terminal aggregations. Furthermore, the molecular geometry that is affected by the mesomeric configurations also affects the molecular-molecular interactions. In our previous studies, we concluded that the molecular aggregation of rod-like molecules by the lateral attraction of planar molecules enforced with longer alkenyl-chains might play the main role in the mesophase activity of LC compounds with two aromatic rings [2,30]. Another factor is the end-to-end association of terminal flexible chains that differs according to mesomeric effects. These factors combine in different ratios to affect the mesomorphic properties. From the viewpoint of entropy, a dominant role of the alkenyl chains is their liability, and that they can easily make multi-conformational changes [45]. Thus, the lower values of estimated entropy changes for conventional low molar mass mesogens may be attributed to the thermal cis-trans isomerization of the CH=N linkage, which is in agreement with previous reports [33,46–48].

3.2. Measurements of Refractive Index

Abbe refractometer, made by Bellingham, England, with a heating control unit thermostat within ±0.1 °C around the prisms, was used for measuring the refractive index at certain degrees of temperature. The compound was exposed to a sodium lamp (589.3 nm). In order to measure the ordinary and extraordinary refractive indices (no and ne) of the liquid crystalline sample, the prisms of Abbe refractometer were modulated in planar and homeotropic alignments, respectively. The values of no and ne for the compound (**I**) were taken during the cooling process with the accuracy of ±0.0005, as shown in Figure 4. It was clear that as the temperature increases, the no values increase and the ne values decrease.

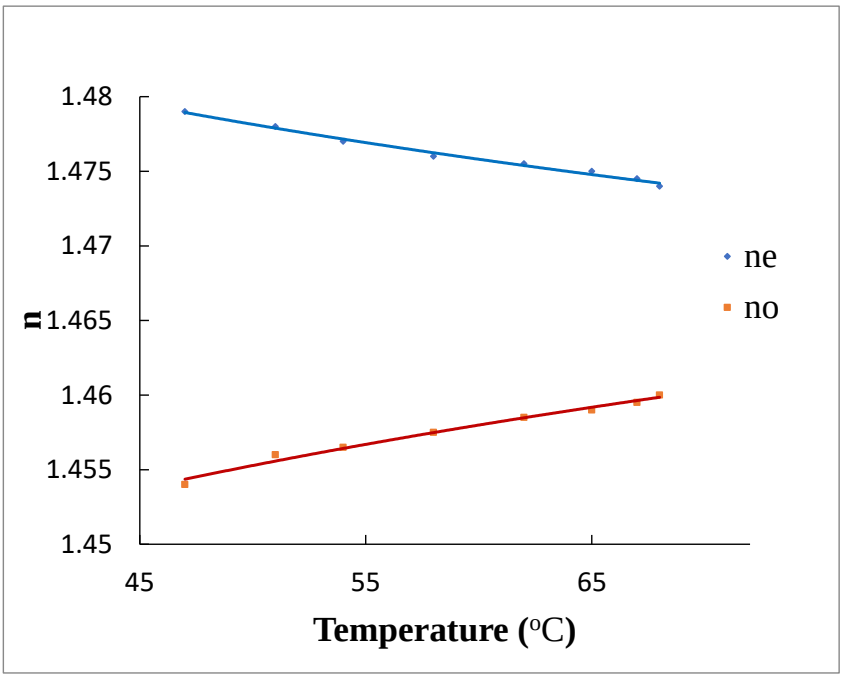

Figure 4. Temperature dependence of refractive indices n_o and n_e for compound **I** at 589.3 nm.

The effective geometry α_{eg} is the dispersion of light in liquid crystals that can be obtained by the following equation [49–51]:

$$\alpha_{eg} = \frac{n_o}{n_e} \quad (1)$$

Figure 5 shows that for compound **I**, the α_{eg} values increase with increasing mesomorphic temperature. The α_{eg} values reach unity in the isotropic phase because the molecular orientation order in the sample used vanished [52,53].

3.3. Measurements for Birefringence

3.3.1. Birefringence Measurement using the Abbe Refractometer

One of the critical parameters that affects the operation of electro-optic devices is the birefringence of the liquid crystal [50,53,54]. Figure 6 describes the values of birefringence (Δ), which is the difference between the measuring n_e and n_o for compound **I** at different temperatures using a sodium lamp 589.3 nm. It has been noted that as the temperature increases, Δn gradually decreases [50–57]. Figure 6 describes the best curve fitting of Δn values using the Cauchy dispersion relationship.

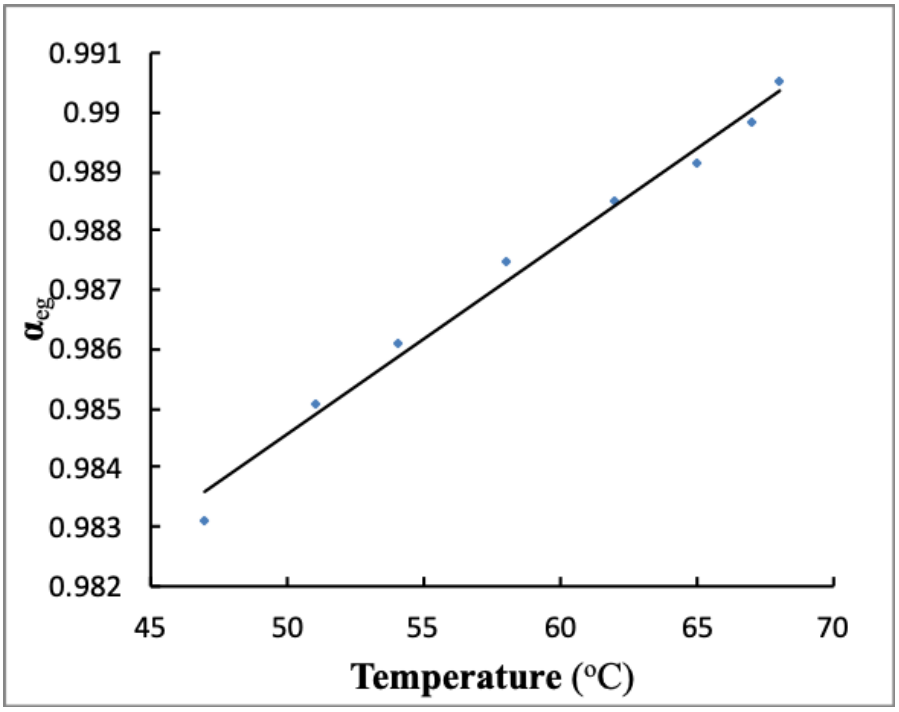

Figure 5. The parameter of effective geometry α_{eg} varies with temperature for the investigated compound, **I**.

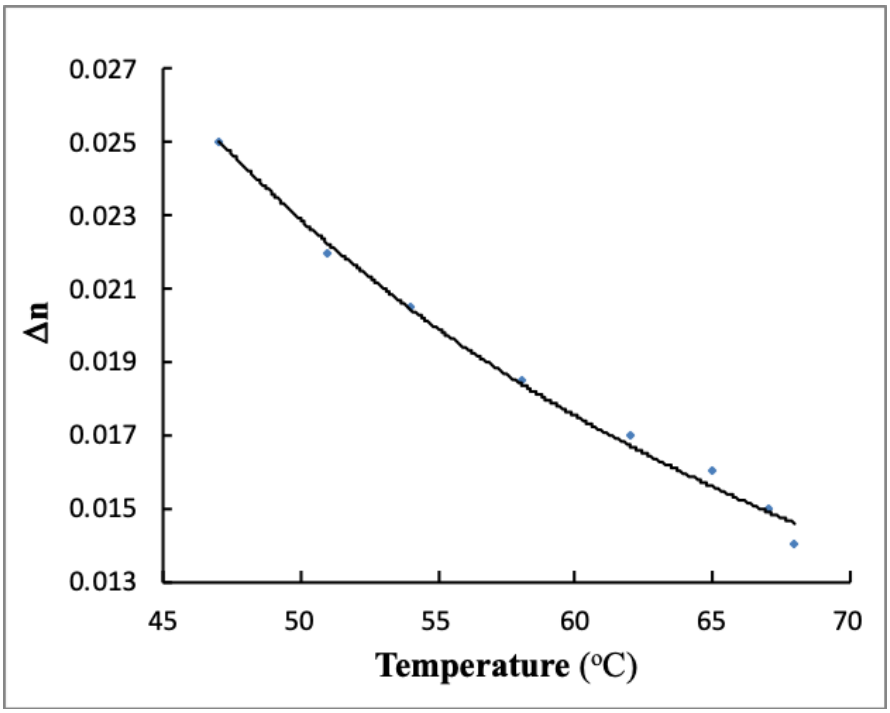

Figure 6. Temperature dependence of birefringence at 589.3 nm. The dots represent the measured birefringence Δn, and the solid line refers to the fitting using the relation of Cauchy dispersion.

3.3.2. Birefringence Measurement by a Modified Spectrophotometer

The phase transition temperature and birefringence for mesomorphic materials can be obtained during heating and cooling from the transmission spectrum by the modified spectrophotometer (MS)

method as in Figure 7 [56,57]. The setup consists of the diffraction grating D, rotating disc R, mirror M, beam splitter B, and P_1 and P_2 as a polarizer and analyzer. The sample S was placed between two glass slices with two polarizers and positioned in the electric oven with a heating control unit of rate 1 °C/min, as in Figure 7. The transmitted light intensity was measured as a function of the wavelength (200–900 nm) at a specific temperature using the MS technique.

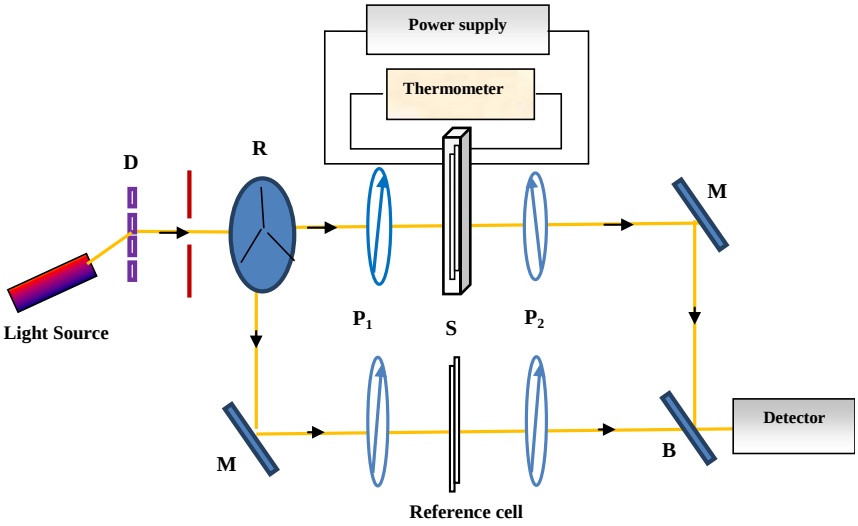

Figure 7. Optical set-up of spectrophotometry for measuring the transition temperatures of liquid crystalline materials, where D: diffraction grating; R: rotating disc (Sample, blank, shutter); M: mirror; B: beam splitter; P_1 and P_2 are polarizer and analyzer respectively; S: sample inside the electric oven.

Figure 8 shows the difference of light transmittance with wavelength at certain temperatures through the cooling action of the sample **I** placed between two crossed polarizers. The transmittance change occurs due to the compound mesogens orientation. Using the MS method, the transition temperatures were determined, and the results obtained were compatible with those determined by DSC and POM techniques.

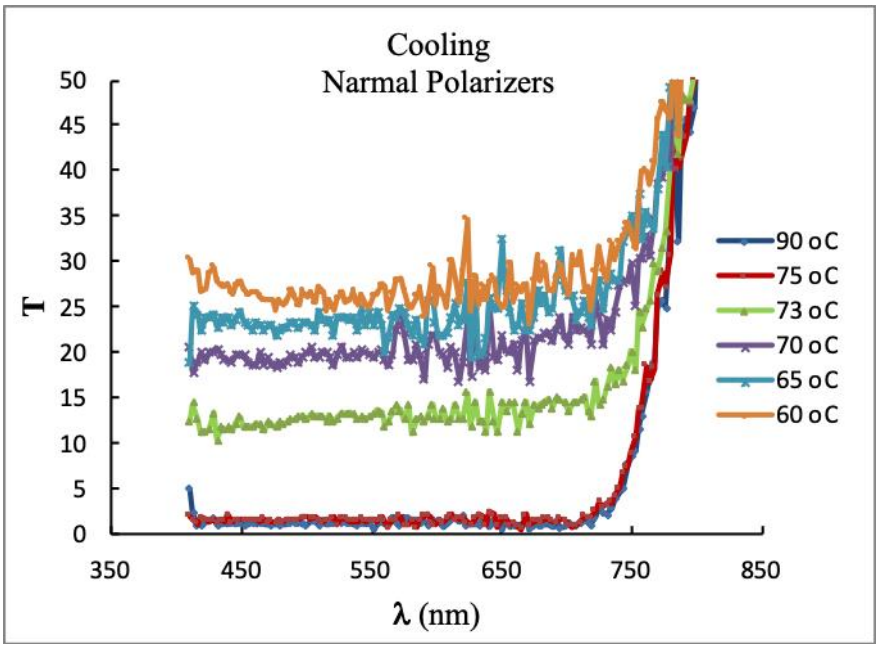

Figure 8. The variable transmittance with wavelength at certain temperatures for the prepared compound (**I**).

Birefringence (Δn) was measured in the LC phase from the light transmission of the sample as follows [56–59]:

$$\Delta n = \frac{\lambda}{\pi t} sin^{-1} \sqrt{\frac{T_{\perp}(\lambda)}{T_{\parallel}(\lambda)}} \quad (2)$$

where $T_{\perp}$ and $T_{\parallel}$ represent the transmittance of light in crossed and parallel polarizers, respectively. Using the MS method, the $T_{\perp}$ and $T_{\parallel}$ values at specific wavelength and temperature were determined for compound **I**. A traveling microscope was used to determine the thickness t of a sample and was equivalent to 30 μm.

The values of Δn of compound **I** in the LC phase at specific temperature with wavelength 589.3 nm were estimated and compared with that obtained using the Abbe refractometer as shown in Table 2.

Table 2. The birefringence Δn by using the modified spectrophotometer (MS), Abbe refractometer and interferometric techniques at 589.3 nm and temperature of 65 °C, Δn_o is the birefringence at T = 0 °C and the material constant β for the investigated compound.

Sample	Δn (MS)	Δn (Abbe Refractometer)	Δn (Interferometric)	Δn_o	β
I	0.018 ± 0.005	0.017 ± 0.005	0.022 ± 0.005	0.031 ± 0.005	0.01

3.3.3. Interferometric Method

The interferometric method was based on interference of linearly polarized light travelling through birefringent medium and exploiting linear or circular polariscope [60–62].

The intensity I of the light leaving the polariscope after passing through the liquid crystal cell was given as follows [63–66]:

$$I = 2I_o T^2 \left[cos^2\left(\theta_p - \theta_a\right) - sin\left(2\theta_p\right) sin(2\theta_a) sin^2\left(\frac{\pi t \Delta n}{\lambda}\right)\right] \quad (3)$$

where I_o is the intensity of the incident monochromatic light of wavelength λ on the polariscope, T is the transmission of a linear polariscope, θ_p and θ_a are the angles between axes of transmission of polarizer and analyzer, which are measured in the plane of the principal section of the liquid crystal cell, Δn is the birefringence, and t is the thickness of the sample.

When θ_p = +45° and θ_a = −45° or inversely θ_p = −45° and θ_a = +45°, which means that the polarizer and analyzer are perpendicular to each other, Equation (3) becomes:

$$I = 2I_o T^2 sin^2\left(\frac{\pi t \Delta n}{\lambda}\right) = I_m sin^2\left(\frac{\pi t \Delta n}{\lambda}\right) \quad (4)$$

where $I_m = 2I_o T^2$.

So that:

$$\Delta n = \frac{\lambda}{\pi t} sin^{-1} \sqrt{\frac{I}{I_m}} \quad (5)$$

By measuring the intensities, I and I_m, the value of Δn could be obtained by knowing the wavelength λ and the thickness t as shown in Table 2.

3.4. Order Parameter Measurement

By applying the hypothesis of Vuks, the microscopic order parameter **S** was determined from the measured values of n_e and n_o for the investigated compound **I** as follows [67]:

$$S\left(\frac{\Delta\alpha}{\alpha}\right) = \frac{\left(n_e^2 - n_o^2\right)}{\langle n^2 \rangle - 1} \quad (6)$$

where $\Delta\alpha$ and α are, respectively, the anisotropic and mean molecular polarizability, and $\langle n^2 \rangle$ is the mean square value of the refractive index. By using the extrapolation method of Haller, the scaling factor $\Delta\alpha/\alpha$ is obtained, and replacing it with Equation (6), the parameter ***S*** can be estimated for the compound **I** [56,57,68].

In the crystalline and mesophase phase, the macroscopic order parameter Q was related to the birefringence Δn and Δn_o, as follows [69,70]:

$$Q = \frac{\Delta n}{\Delta n_o} \tag{7}$$

The Haller formula can be used to obtain the value of Δn_o as follows [56–58]:

$$\Delta n = \Delta n_o \left(1 - \frac{T}{T_c}\right)^{\beta} \tag{8}$$

where T_C is the transition temperature from the smectic A to isotropic, and β is a constant of the material. The values of Δn_o and β were determined from the relationship between Δn and $Ln\ (1 - T/T_C)$, as listed in Table 2. Figures 9 and 10 show that the relationship between ***S*** and Q for compound **I** with temperature is inversely proportional; however, the relation with Δn appears linearly. It was noted that the ***S*** and Q values for compound **I** are nearly the same.

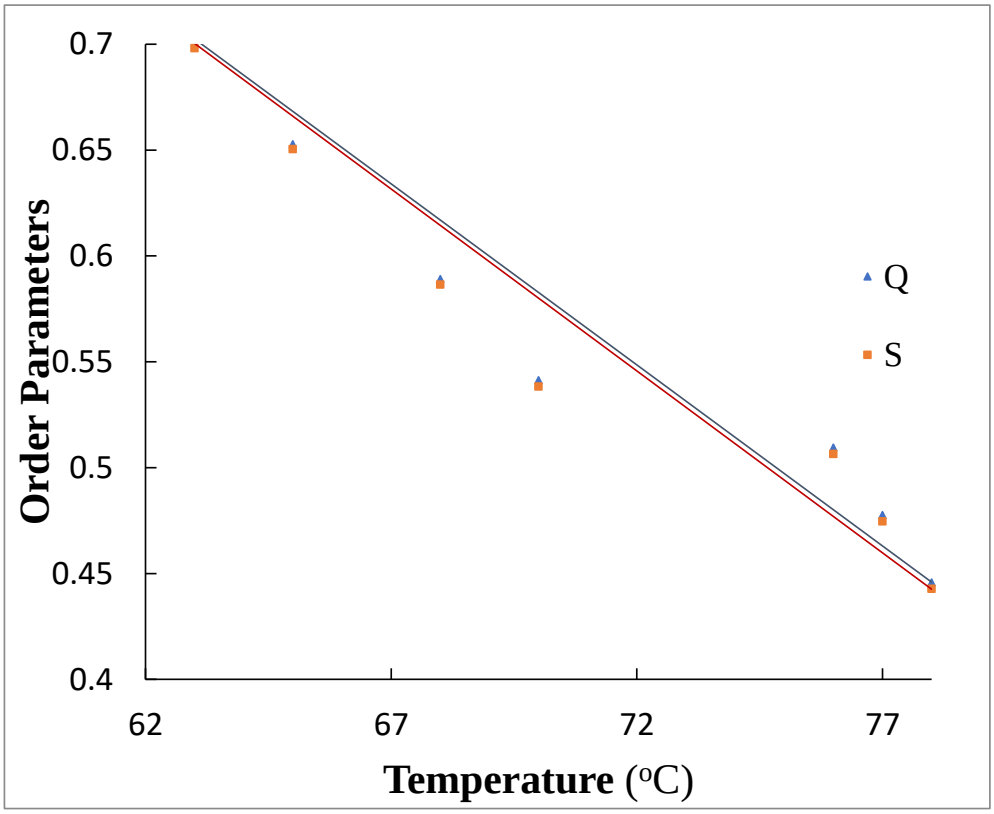

Figure 9. The relationship between parameters (Q and ***S***) and temperature for compound **I**.

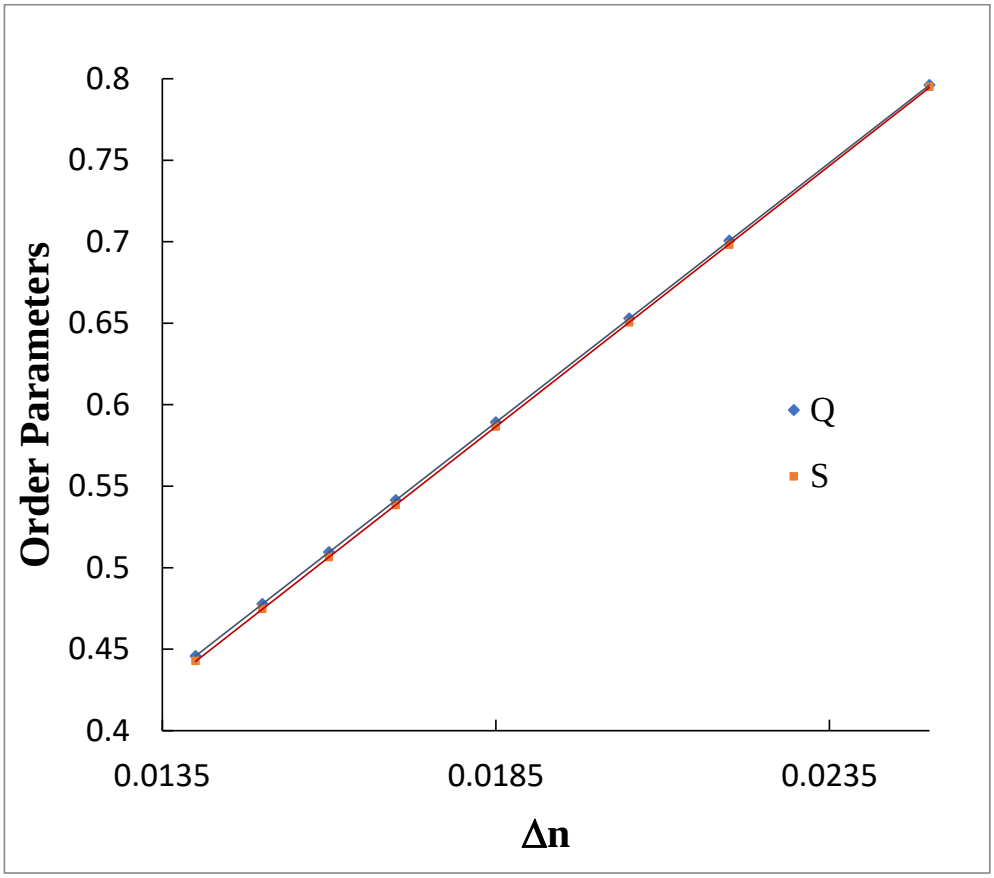

Figure 10. The variability of the microscopic parameters (Q and *S*) with birefringence (Δn).

3.5. Molecular Polarizability

Molecular polarizability for liquid crystal materials is a significant parameter. The ordinary (α_o) and extraordinary (α_e) polarizability describe the electrical vector perpendicularly and parallel to the optical axis of the mesomorphic compound **I**, and can be calculated by the method of Vuks as follows [56]:

$$\alpha_e = \left(\frac{3}{4\pi N}\right)\left(\frac{n_e^2 - 1}{\langle n^2\rangle + 2}\right) \quad (9)$$

$$\alpha_o = \left(\frac{3}{4\pi N}\right)\left(\frac{n_o^2 - 1}{\langle n^2\rangle + 2}\right) \quad (10)$$

where N is the number of molecules per volume, and $\langle n^2 \rangle$ is the refractive index mean square value, which is given as follows [56,71]:

$$\langle n^2\rangle = \frac{n_e^2 + 2n_o^2}{3} \quad (11)$$

The α_e and α_o values for the prepared compound **I** with variable temperature are presented in Figure 11. The α_e values increase as the temperature decreases, while α_o values increase with increasing temperature. This α_e and α_o temperature dependence shows the same behavior as birefringence. Moreover, α_e/α_o values have linear dependency with temperature (Figure 12).

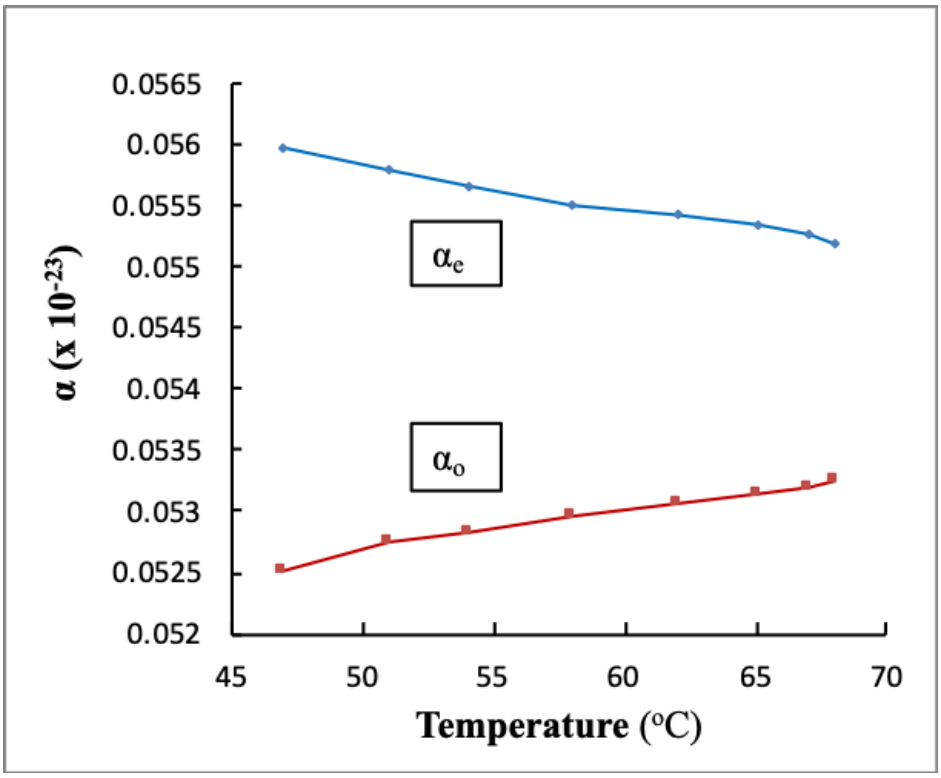

Figure 11. The relationship between the molecular polarizability and temperature for compound **I**.

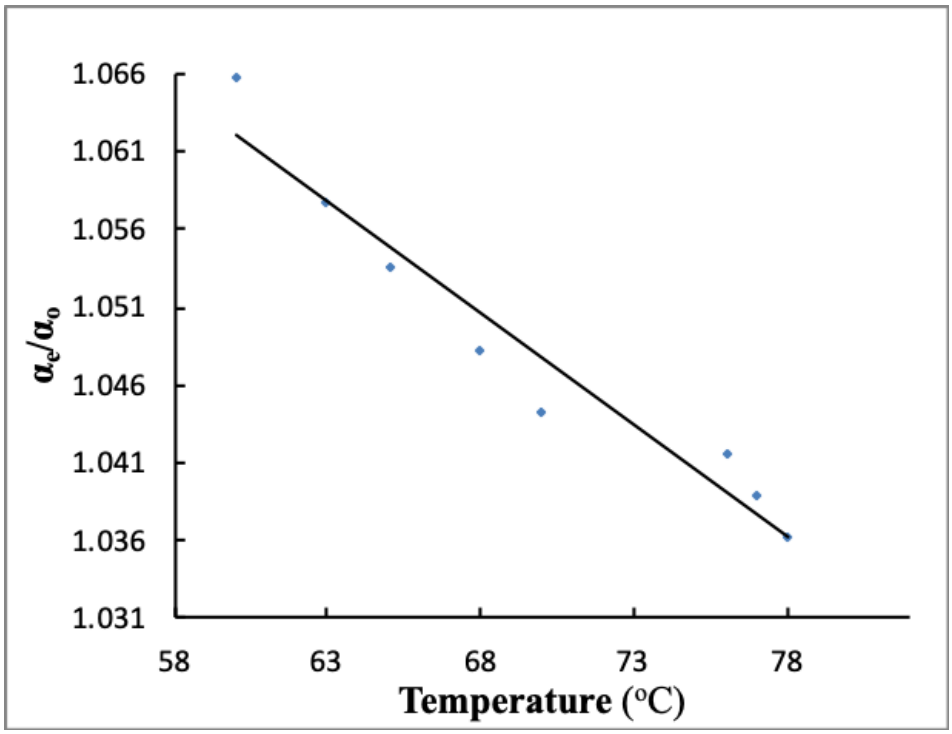

Figure 12. The relationship between the molecular polarizability and temperature for compound **I**.

3.6. Molecular Modeling (DFT Calculations)

Three configurational isomers are proposed according to the orientation of the -CH=N- group with respect to the MeO and the C=O of the carboxylate as follows, Figure 13:

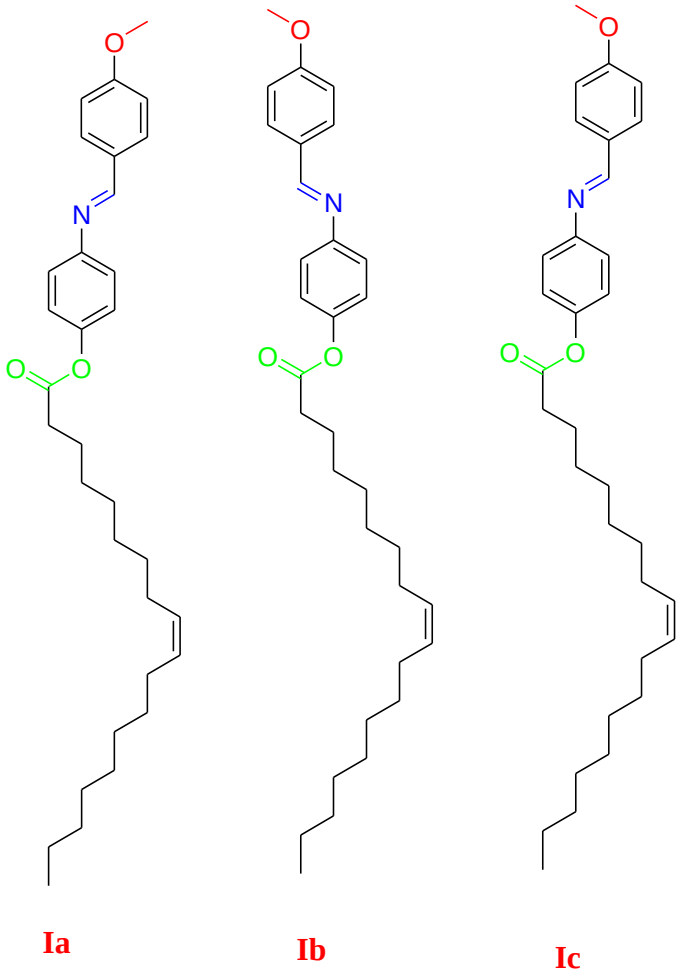

Figure 13. The proposed configurational isomers (**Ia**–**c**) of the prepared compound **I**.

3.6.1. Molecular Geometry

Three geometrical isomers of the prepared compound (**I**) were investigated to predict the most stable isomer (**Ia**–**c**). These isomers were built according to the orientation of the -CH=N- with respect to the $–OCH_3$ and the carbonyl group of the –COO- linkage of the oleate moiety. The DFT calculations were carried out to estimate the stability of the proposed isomers (**Ia**–**c**). The theoretical DFT calculations were carried out in gas phase at B3LYP 6-311G(d,p) basis set. The absence of the imaginary frequency for all suggested conformers is proof of their stability, Figure 14.

Table 3 shows selected structural parameters of the optimum geometries of the postulated isomers. The twist angles between the two phenyl rings were estimated. The twist angle for all estimated isomers are strongly affected by the orientation of the -CH=N- linkage with respect to the terminal groups. The twist angle was 49.1, 48.5 and 55.4° for the isomers **Ia**, **Ib** and **Ic**, respectively. Isomer **Ib** showed the most planar geometry with the least twist angle; however, **Ic** had the least planarity. Such planarity could affect the degree of packing of the molecules in the condensed liquid crystalline phase. Moreover, the co-planarity of the liquid crystals is an essential parameter affecting the mesophase behavior [38]. On the other hand, the estimated aspect ratio of the proposed compounds has been calculated from the predicted dimensional parameters. It was clear that the orientation of the -CH=N- linkage does not significantly affect the aspect ratio of the proposed isomers.

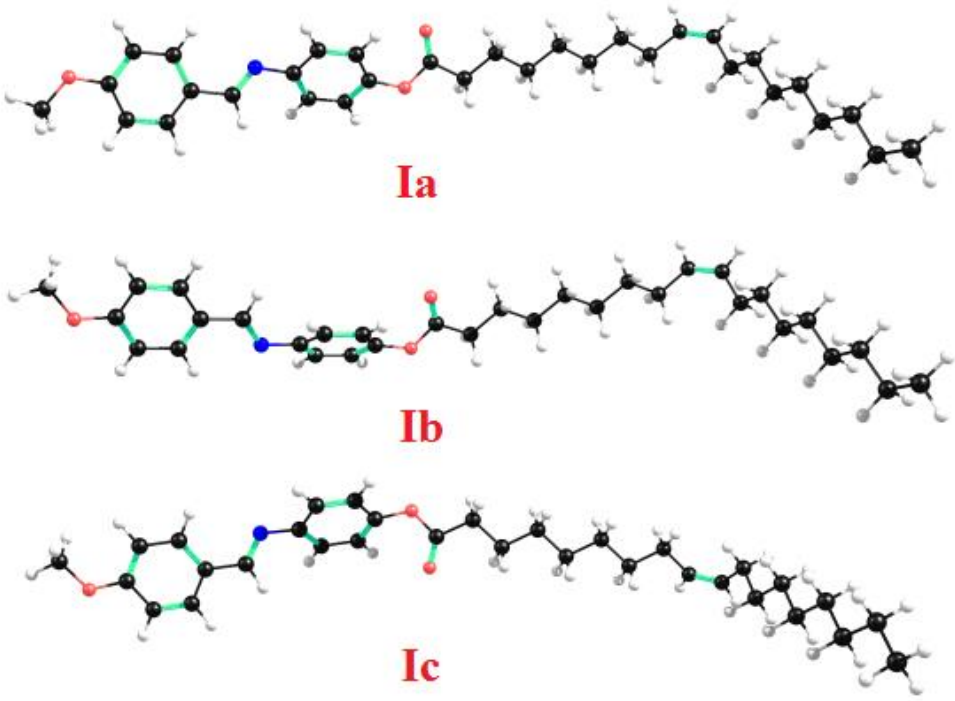

Figure 14. Calculated molecular geometry of the proposed configurational isomers, **Ia–c**.

Table 3. Dimensional parameters and aspect ratios of estimated geometrical isomers of **I**.

Parameter		Ia	Ib	Ic
Dimensions Å	**Width (D)**	33.0	32.0	32.0
	Length (L)	13.1	13.4	13.2
Aspect ratio (L/D)		2.5	2.4	2.4
Twist angle (Degree)		49.1	48.5	55.4
Dipole moment, (Debye)		3.4804	3.9182	2.1570
Polarizability, (Bohr^3)		427.12	425.09	402.11

The dipole moment and polarizability of the investigated isomers were calculated using the same method. Both the dipole moment as well as the polarizability of the isomers were significantly affected by the geometrical orientation of the mesogenic group (C=N) with respect to the terminal groups. The configurational structure greatly affected the polarity and highly impacted the polarizability of the molecules. Isomers **Ia** and **Ib** showed almost the same dipole moment and polarizability; however, the other isomer **Ic** differed by almost 20 Bohr^3 in the polarizability and by 1.5 Debye in the dipole moment. These results can be explained in terms of the co-planarity of the aromatic rings.

Thermal parameters calculated by the same method at the same base site are summarized in Table 4. The results of the theoretical calculations for the three geometrical isomers, **Ia–c**, revealed that the conformer **Ia** of the highest co-planar aromatic core is the most stable conformer; however, **Ic** of the least co-planar isomer is the least stable, with an energy difference of 209 K cal mol^{-1}. In contrast, the energy difference between the **Ia** and **Ib** isomers is 0.3 K cal mol^{-1}. The lower energy difference between the more stable isomers **Ia** and **Ib** is evidence of their interconverting equilibrium. The high stability of the conformer **Ib** could be attributed to the geometrical parameter results that may permit the high degree of aromatic co-planarity.

Table 4. Thermal parameters (Hartree/Particle) of estimated geometrical isomers, **Ia–c**.

Parameter	Ia	Ib	Ic
$\mathbf{E_{corr}}$	0.706	0.706	0.710
ZPVE	−1526.629	−1526.630	−1526.295
$\mathbf{E_{tot}}$	−1526.589	−1526.590	−1526.255
H	−1526.588	−1526.589	−1526.254
G	−1526.713	−1526.714	−1526.378
ΔE (Kcal/mole)	0.3	0.0	209.8

Abbreviations: ZPVE: Sum of electronic and zero-point energies; E_{tot}: Sum of electronic and thermal energies; H: Sum of electronic and thermal enthalpies; G: Sum of electronic and thermal free energies.

3.6.2. Frontier Molecular Orbitals (FMOs)

Table 5 and Figure 15 present the estimated plots of frontier molecular orbitals HOMO (highest occupied) and LUMO (lowest unoccupied) of all postulated configurational isomers **Ia–c** of the prepared compound, **I**. As shown in the figure, it is clear that the electron densities of the sites that shared in the formation of the HOMOs and the LUMOs are localized on the aromatic rings. Moreover, there was no obvious impact of the geometrical configuration of the mesogenic core or the terminal chains on the location of the electron densities of the FMOs. However, the orientation of the groups insignificantly affects the energy gap between the FMOs. The configuration of the investigated groups of the isomer **Ic** increases the energy level of the FMOs. The predicted energy gap between the FMOs could be used in the estimate of the capability of electron transfer between the FMOs during any electronic excitation process. The global softness (**S**) = **1/ΔE** is the parameter that shows the degree of polarizability of materials as well as their photoelectric sensitivity.

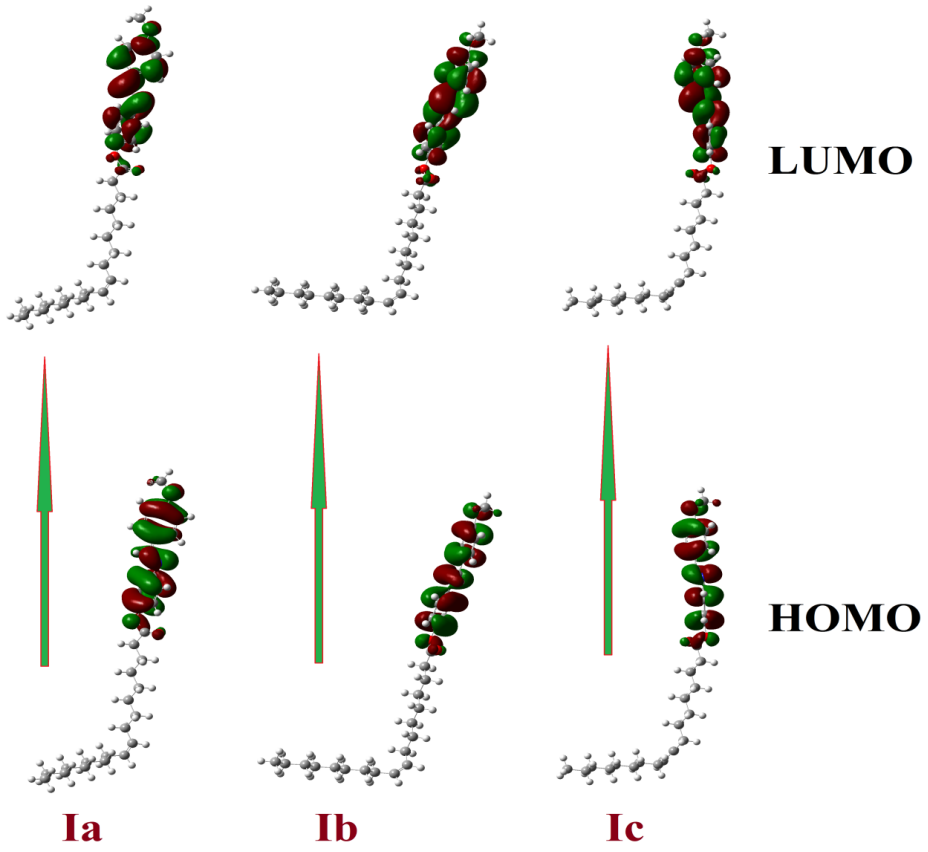

Figure 15. The estimated plots for frontier molecular orbitals of all isomers **Ia–c**.

Table 5. Frontier molecular orbital (FMO) energies a.u., and softness of all isomers (**Ia–c**).

Parameter	Ia	Ia	Ic
E_{LUMO}	−0.05920	−0.05897	−0.05128
E_{HOMO}	−0.21328	−0.21342	−0.20452
$\Delta E_{HOMO-LUMO}$	0.154	0.154	0.153
S Softness	6.490	6.475	6.526

3.6.3. MEP Analysis

The charge distribution map for the proposed conformers **Ia–c** was calculated under the same basis sets according to the molecular electrostatic potential (MEP, Figure 16). The red region (negatively charged atomic sites) was distributed on the aromatic rings and the maximum was on the carbonyl group of ester linkage for all isomers, while the methoxy groups are the least negatively charged atomic sites (blue regions). As shown in Figure 16, there are significant effects of the orientation of the C=N group compared to the C=O and OMe groups on the mapping of the charge destitution. Since the stability of the enhanced mesophase and other mesomorphic properties are highly impacted by the degree of packing of the compounds, which is affected by the geometrical structure, the orientation of the charge distribution could have an impact on this property.

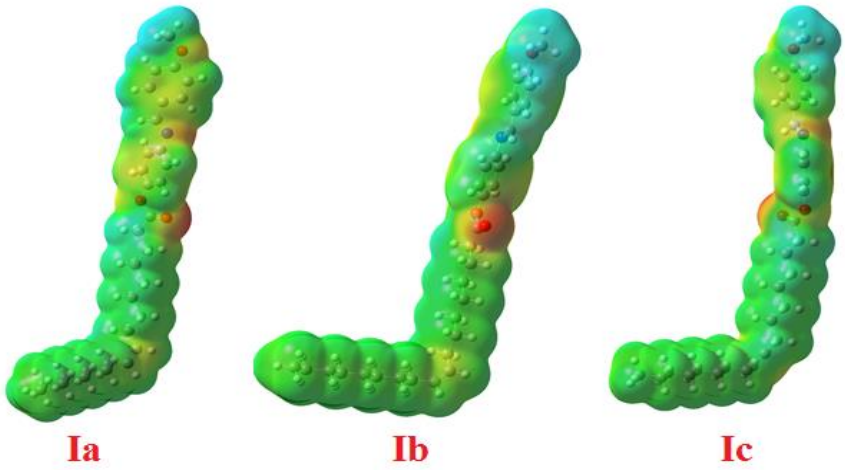

Figure 16. Molecular electrostatic potentials (MEP) for all investigated isomers, **Ia–c**.

4. Conclusions

Herein, thermotropic mono-azomethine liquid crystalline material based on a natural fatty acid derivative, operating in region near to the room-temperature, has been synthesized and characterized experimentally and theoretically. The mesomorphic and optical behavior were investigated and the computational approaches were established to confirm the experimental data, which was produced using DFT calculations. Moreover, ordinary/extraordinary refractive indices and the birefringence with different temperatures were analyzed and briefly discussed. The results show that the investigated material possesses an enantiotropic monomorphic phase comprising a smectic A phase within the near to room-temperature range. The geometrical isomerism affects many thermal parameters such as aspect ratio, planarity and dipole moment. Thermal parameters of the theoretical calculations revealed that the highest co-planar aromatic core (**Ia**) is the most stable conformer. The same dipole moment and polarizability were shown for isomers **Ia** and **Ib**; however, the other isomer **Ic** differed by almost 20 $Bohr^3$ in the polarizability and by 1.5 Debye in the dipole moment.

Supplementary Materials: The following are available online at http://www.mdpi.com/2073-4352/10/11/1044/s1, Table S1. ^{1}H-NMR chemical shifts, Figure S1. ^{1}H-NMR of (4-methoxybenzylideneamino)phenyl oleate at 305 K. Figure S2. ^{13}C-NMR of (4-methoxybenzylideneamino)phenyl oleate at 305 K. Figure S3. HSQC-NMR of (4-methoxybenzylideneamino)phenyl oleate at 305 K. Figure S4. ^{1}H-NMR of (4-methoxybenzylideneamino)phenyl oleate at 310 K. Figure S5. ^{1}H-NMR of (4-methoxybenzylideneamino)phenyl oleate at 315 K. Figure S6. ^{1}H-NMR of (4-methoxybenzylideneamino)phenyl oleate at 320 K. Figure S7. ^{1}H-NMR of (4-methoxybenzylideneamino)phenyl oleate at 325 K. Figure S8. ^{1}H-NMR of (4-methoxybenzylideneamino)phenyl oleate at 335 K. Figure S9. ^{1}H-NMR of (4-methoxybenzylideneamino)phenyl oleate at 345 K. Figure S10. ^{1}H-NMR of (4-methoxybenzylideneamino)phenyl oleate at 355 K. Figure S11. ^{1}H-NMR of (4-methoxybenzylideneamino)phenyl oleate at 365 K.

Author Contributions: Data curation, A.A.Z., H.A.A., M.H. and R.B.A.; Formal analysis, M.H. and A.-H.E.; Funding acquisition, A.A.Z., R.B.A. and A.-H.E.; Investigation, A.A.Z., H.A.A. and M.H.; Methodology, A.A.Z., H.A.A. and M.H.; Project administration, R.B.A. and M.J.; Resources, A.A.Z., H.A. and M.J.; Software, M.H.; Supervision, A.A.K.; Validation, H.A.; Writing—original draft, A.A.Z., M.H. and A.-H.E.; Writing—review and editing, H.A.A. and M.H. All authors have read and agreed to the published version of the manuscript.

Funding: This research received no external funding.

Conflicts of Interest: The authors declare no conflict of interest.

References

1. Seredyuk, M.; Gaspar, A.B.; Ksenofontov, V.; Reiman, S.; Galyametdinov, Y.G.; Haase, W.; Rentschler, E.; Gütlich, P. Room Temperature Operational Thermochromic Liquid Crystals. *Chem. Mater.* **2006**, *18*, 2513–2519. [CrossRef]
2. Hagar, M.; Ahmed, H.A.; Alhaddad, O.A. New azobenzene-based natural fatty acid liquid crystals with low melting point: Synthesis, DFT calculations and binary mixtures. *Liq. Cryst.* **2019**, *46*, 2223–2234. [CrossRef]
3. Pramanik, A.; Das, M.K.; Das, B.; Żurowska, M.; Dąbrowski, R. Electro-optical properties of a new series of fluorinated antiferroelectric orthoconic liquid crystalline esters. *Liq. Cryst.* **2015**, *42*, 412–421. [CrossRef]
4. Heilmeier, G.; Zanoni, L.; Barton, L. Dynamic scattering: A new electrooptic effect in certain classes of nematic liquid crystals. In *Proceedings of the Proceedings of the IEEE*; Institute of Electrical and Electronics Engineers (IEEE): Piscataway, NJ, USA, 1968; Volume 56, pp. 1162–1171.
5. Goodby, J. *Ferroelectric Liquid Crystals. Principles, Properties and Applications*; Ferroelectricity and related Phenomena Series; Gordon & Breach: London, UK, 1992; Volume 7, p. 496. [CrossRef]
6. Carlton, R.J.; Hunter, J.T.; Miller, D.S.; Abbasi, R.; Mushenheim, P.C.; Na Tan, L.; Abbott, N.L. Chemical and biological sensing using liquid crystals. *Liq. Cryst. Rev.* **2013**, *1*, 29–51. [CrossRef] [PubMed]
7. Wang, M.; Cao, R.; Zhang, L.; Yang, X.; Liu, J.; Xu, M.; Shi, Z.; Hu, Z.; Zhong, W.; Xiao, G. Remdesivir and chloroquine effectively inhibit the recently emerged novel coronavirus (2019-nCoV) in vitro. *Cell Res.* **2020**, *30*, 269–271. [CrossRef]
8. Shvartsman, F.; Krongauz, V. Quasi-liquid crystals. *Nat. Cell Biol.* **1984**, *309*, 608–611. [CrossRef]
9. Aleksandriiskii, V.V.; Novikov, I.V.; Kuvshinova, S.A.; Burmistrov, V.A.; Koifman, O.I. Dielectric, optical and orientational properties of liquid crystalline 4-alkyloxy-4′-cyanoazoxybenzenes and 4-alkyloxy-4′-cyanoazobenzenes. *J. Mol. Liq.* **2016**, *223*, 1270–1276. [CrossRef]
10. De Gennes, P.G.; Prost, J. *The Physics of Liquid Crystals*, 2nd ed.; International Series of Monographs on Physics; Oxford Science Publication: Oxford, UK, 1993; Volume 83, ISBN 13 978-0198517856.
11. Kumar, S. Liquid Crystals: Experimental Study of Physical Properties and Phase Transitions. *Molecules* **2001**, *6*, 1055–1056. [CrossRef]
12. Priestly, E. *Introduction to Liquid Crystals*; Springer Science & Business Media: Princeton, UK, 2012.
13. Ahmed, H.A.; Khushaim, M.S. Nematic Phase Induced from Symmetrical Supramolecular H-Bonded Systems Based on Flexible Acid Core. *Crystals* **2020**, *10*, 801. [CrossRef]
14. Ahmed, H.A.; Khushaim, M.S. Nematogenic Laterally Substituted Supramolecular H-Bonded Complexes Based on Flexible Core. *Crystals* **2020**, *10*, 878. [CrossRef]
15. Al-Mutabagani, L.A.; Ahmed, H.A.; Hagar, M.; Alshabanah, L.A. Experimental and computational approaches of newly polymorphic supramolecular H-bonded liquid crystal complexes. *Front. Chem.* **2020**, *8*, 930. [CrossRef]
16. Szulc, J.; Stolarz, Z. The Investigation of the Thermal Stability of Liquid Crystals. *Mol. Cryst. Liq. Cryst. Sci. Technol. Sect. A Mol. Cryst. Liq. Cryst.* **1995**, *263*, 623–633. [CrossRef]
17. Kelker, H.; Scheurle, B. Eine flüssig-kristalline (nematische) Phase mit besonders niedrigem Erstarrungspunkt. *Angew. Chem.* **1969**, *81*, 903–904. [CrossRef]

18. Gray, G.W.; Vill, V.; Spiess, H.W.; Demus, D.; Goodby, J.W. *Physical Properties of Liquid Crystals*; John Wiley & Sons: Hoboken, NJ, USA, 2009. [CrossRef]
19. Raal, J.D. An Analysis of Conductive Heat Losses in a Flow Calorimeter for Heat Capacity Measurement. In *Heat Capacities*; Chapter 3; Royal Society of Chemistry (RSC): London, UK, 2010; pp. 41–53.
20. Ogura, I. Low dielectric constant epoxy resins. In *Handbook of Low and High Dielectric Constant Materials and Their Applications*; Elsevier: Amsterdam, The Netherlands, 1999; Volume 1, pp. 213–240. [CrossRef]
21. Yildiz, S.; Özbek, H.; Glorieux, C.; Thoen, J. Critical behaviour at the isotropic–nematic and nematic–smectic A phase transitions of 4-butyloxyphenyl 4′-decyloxybenzoate liquid crystal from refractive index data. *Liq. Cryst.* **2007**, *34*, 611–620. [CrossRef]
22. Gramsbergen, E.F.; De Jeu, W.H. First- and second-order smectic-A to nematic phase transitions in p,p?-dialkylazoxybenzenes studied by birefringence. *J. Chem. Soc. Faraday Trans. 2 Mol. Chem. Phys.* **1988**, *84*, 1015. [CrossRef]
23. Nesrullajev, A. Texture transformations and thermo-optical properties of nematic mesogen at nematic–isotropic liquid phase transition. *J. Mol. Liq.* **2014**, *196*, 217–222. [CrossRef]
24. Zaki, A. Optical measurements of mixture thermotropic liquid crystals. *Opt. Lasers Eng.* **2010**, *48*, 538–542. [CrossRef]
25. El-Dessouki, T.A.; Roushdy, M.; Hendawy, N.I.; Naoum, M.M.; Zaki, A.A. Optical Measurements of Thermotropic Liquid Crystals. *J. Mod. Phys.* **2013**, *4*, 39–48. [CrossRef]
26. Zaki, A.A. Optical Measurements and Speckle Photography for Thermotropic Liquid Crystals Mixtures. *J. Mod. Phys.* **2013**, *4*, 517–521. [CrossRef]
27. Yeap, G.-Y.; Hng, T.-C.; Yeap, S.-Y.; Gorecka, E.; Ito, M.M.; Ueno, K.; Okamoto, M.; Mahmood, W.A.K.; Imrie, C.T. Why do non-symmetric dimers intercalate? The synthesis and characterisation of the α-(4-benzylidene-substituted-aniline-4′-oxy)-ω-(2-methylbutyl-4′-(4″-phenyl)benzoateoxy)alkanes. *Liq. Cryst.* **2009**, *36*, 1431–1441. [CrossRef]
28. Yeap, G.-Y.; Lee, H.-C.; Mahmood, W.A.K.; Imrie, C.T.; Takeuchi, D.; Osakada, K. Synthesis, thermal and optical behaviour of non-symmetric liquid crystal dimers α-(4-benzylidene-substituted-aniline-4′-oxy)-ω-[pentyl-4-(4′-phenyl)benzoateoxy]hexane. *Phase Transit.* **2011**, *84*, 29–37. [CrossRef]
29. Yeap, G.-Y.; Osman, F.; Imrie, C.T. Non-symmetric dimers: Effects of varying the mesogenic linking unit and terminal substituent. *Liq. Cryst.* **2015**, *42*, 543–554. [CrossRef]
30. Alnoman, R.; Al-Nazawi, F.K.; Ahmed, H.A.; Hagar, M. Synthesis, Optical, and Geometrical Approaches of New Natural Fatty Acids' Esters/Schiff Base Liquid Crystals. *Molecules* **2019**, *24*, 4293. [CrossRef] [PubMed]
31. Paterson, D.A.; Crawford, C.A.; Pociecha, D.; Walker, R.; Storey, J.M.; Gorecka, E.; Imrie, C.T. The role of a terminal chain in promoting the twist-bend nematic phase: The synthesis and characterisation of the 1-(4-cyanobiphenyl-4′-yl)-6-(4-alkyloxyanilinebenzylidene-4′-oxy)hexanes. *Liq. Cryst.* **2018**, *45*, 2341–2351. [CrossRef]
32. Bhola, G.N.; Bhoya, U.C. Molecular structural flexibility dependence of mesomorphism through ortho-substituted bromo group. *Mol. Cryst. Liq. Cryst.* **2016**, *630*, 188–196. [CrossRef]
33. Henderson, P.A.; Imrie, C.T. Methylene-linked liquid crystal dimers and the twist-bend nematic phase. *Liq. Cryst.* **2011**, *38*, 1407–1414. [CrossRef]
34. Yeap, G.-Y.; Ha, S.-T.; Lim, P.-L.; Boey, P.-L.; Mahmood, W.A.K.; Ito, M.M.; Sanehisa, S. Synthesis and Mesomorphic properties of Schiff base esters *Ortho*-hydroxy-*para*-alkyloxybenzylidene-*para*-substituted anilines. *Mol. Cryst. Liq. Cryst.* **2004**, *423*, 73–84. [CrossRef]
35. Vertogen, G.; De Jeu, W.H. *Thermotropic Liquid Crystals, Fundamentals*; Springer Science and Business Media LLC: Princeton, UK, 1988; Volume 45.
36. Foo, K.-L.; Ha, S.-T.; Yeap, G.Y.; Lee, S.L. Mesomorphic behaviors of a series of heterocyclic thiophene-imine-ester-based liquid crystals. *Phase Transit.* **2018**, *91*, 509–520. [CrossRef]
37. Yagai, S.; Kitamura, A. Recent advances in photoresponsive supramolecular self-assemblies. *Chem. Soc. Rev.* **2008**, *37*, 1520–1529. [CrossRef]
38. Hagar, M.; Ahmed, H.; El-Sayed, T.; Alnoman, R. Mesophase behavior and DFT conformational analysis of new symmetrical diester chalcone liquid crystals. *J. Mol. Liq.* **2019**, *285*, 96–105. [CrossRef]
39. Knapkiewicz, M.; Rachocki, A.; Bielejewski, M.; Sebastião, P.J. NMR studies of molecular ordering and molecular dynamics in a chiral liquid crystal with the Sm C α* phase. *Phys. Rev.* **2020**, *101*, 052708.

40. Roy, M.; Jennings, P.A. Real-time NMR Kinetic Studies Provide Global and Residue-specific Information on the Non-cooperative Unfolding of the β-Trefoil Protein, Interleukin-1β. *J. Mol. Biol.* **2003**, *328*, 693–703. [CrossRef]
41. Hagar, M.; Soliman, S.M.; Ibid, F.; El Ashry, E.S.H. Quinazolin-4-yl-sulfanylacetyl-hydrazone derivatives; Synthesis, molecular structure and electronic properties. *J. Mol. Struct.* **2013**, *1049*, 177–188. [CrossRef]
42. Gordon, M.S.; Sojka, S.A.; Krause, J.G. Carbon-13 NMR of para-substituted hydrazones, phenylhydrazones, oximes, and oxime methyl ethers: Substituent effects on the iminyl carbon. *J. Org. Chem.* **1984**, *49*, 97–100. [CrossRef]
43. Paterson, D.A.; Abberley, J.P.; Harrison, W.T.; Storey, J.M.; Imrie, C.T. Cyanobiphenyl-based liquid crystal dimers and the twist-bend nematic phase. *Liq. Cryst.* **2017**, *44*, 1–20. [CrossRef]
44. Meredith, G.R.; VanDusen, J.; Williams, D.J. Optical and nonlinear optical characterization of molecularly doped thermotropic liquid crystalline polymers. *Macromolecules* **1982**, *15*, 1385–1389. [CrossRef]
45. Iam-Choon, K.; Shin-Tson, W. *Optics and Nonlinear Optics of Liquid Crystals*; World Scientific: Philadelphia, PA, USA, 1993; Volume 1.
46. Imrie, C.T.; Karasz, F.E.; Attard, G.S. Comparison of the mesogenic properties of monomeric, dimeric, and side-chain polymeric liquid crystals. *Macromolecules* **1993**, *26*, 545–550. [CrossRef]
47. Donaldson, T.; Staesche, H.; Lu, Z.; Henderson, P.A.; Achard, M.; Imrie, C.T. Symmetric and non-symmetric chiral liquid crystal dimers. *Liq. Cryst.* **2010**, *37*, 1097–1110. [CrossRef]
48. Henderson, P.A.; Niemeyer, O.; Imrie, C.T. Methylene-linked liquid crystal dimers. *Liq. Cryst.* **2001**, *28*, 463–472. [CrossRef]
49. Sastry, S.S.; Rao, B.G.S.; Mallika, K.; Kumari, T.V.; Lakshminarayana, S.; Ha, S.T. Novel method for order parameter of ferroelectric liquid crystals by image analysis. *Liq. Cryst.* **2013**, *40*, 384–390. [CrossRef]
50. Patari, S.; Chakraborty, S.; Nath, A. The optical anisotropy and orientational order parameter of two mesogens having slightly different flexible side chain—A comparative study. *Liq. Cryst.* **2016**, *43*, 1017–1027. [CrossRef]
51. Sastry, S.S.; Kumari, T.V.; Mallika, K.; Rao, B.G.S.; Ha, S.-T.; Lakshminarayana, S. Order parameter studies on EPAP alkanoate mesogens. *Liq. Cryst.* **2012**, *39*, 295–301. [CrossRef]
52. Kumar, A. Determination of orientational order and effective geometry parameter from refractive indices of some nematics. *Liq. Cryst.* **2013**, *40*, 503–510. [CrossRef]
53. Wu, S.-T.; Hsu, C.-S.; Shyu, K.-F. High birefringence and wide nematic range bis-tolane liquid crystals. *Appl. Phys. Lett.* **1999**, *74*, 344–346. [CrossRef]
54. Haller, I. Thermodynamic and static properties of liquid crystals. *Prog. Solid State Chem.* **1975**, *10*, 103–118. [CrossRef]
55. Erkan, S.; Çetinkaya, M.C.; Yildiz, S.; Özbek, H.; Yıldız, S. Critical behavior of a nonpolar smectogen from high-resolution birefringence measurements. *Phys. Rev. E* **2012**, *86*, 041705. [CrossRef]
56. Zaki, A.A.; Ahmed, H.; Hagar, M. Impact of fluorine orientation on the optical properties of difluorophenylazophenyl benzoates liquid crystal. *Mater. Chem. Phys.* **2018**, *216*, 316–324. [CrossRef]
57. Zaki, A.A. Optical measurements of phase transitions in difluorophenylazophenyl benzoate thermotropic liquid crystal with specific orientated fluorine atoms. *Phase Transit.* **2018**, *92*, 135–148. [CrossRef]
58. Uchida, E.; Kawatsuki, N. Photoinduced Orientation in Photoreactive Hydrogen-Bonding Liquid Crystalline Polymers and Liquid Crystal Alignment on the Resultant Films. *Macromolecules* **2006**, *39*, 9357–9364. [CrossRef]
59. Sabirov, L.; Semenov, D. Induced birefringence in the isotropic phase of cholesteric liquid crystals. *Opt. Spectrosc.* **2006**, *101*, 299–302. [CrossRef]
60. Domján, L.; Koppa, P.; Szarvas, G.; Reményi, J. Ternary phase-amplitude modulation with twisted nematic liquid crystal displays for Fourier-plane light homogenization in holographic data storage. *Optik* **2002**, *113*, 382–390. [CrossRef]
61. Tsutsumi, O.; Ikeda, T. Photochemical modulation of alignment of liquid crystals and photonic applications. *Curr. Opin. Solid State Mater. Sci.* **2002**, *6*, 563–568. [CrossRef]
62. Muniandy, S.; Kan, C.; Lim, S.; Radiman, S. Fractal analysis of lyotropic lamellar liquid crystal textures. *Phys. A Stat. Mech. Its Appl.* **2003**, *323*, 107–123. [CrossRef]
63. Pluta, M.; Bisbing, R.E. Advanced Light Microscopy, Vol. 3: Measuring Techniques. *Phys. Today* **1995**, *48*, 56. [CrossRef]
64. Sochacka, M.; Staronski, L.R. Phase-Stepping DIC Technique for Reflecting Surface Evaluation. In *Phase Contrast and Differential Interference Contrast Imaging Techniques and Applications*; International Society for Optics and Photonics: Scotland, UK, 1994; pp. 222–233.

65. Born, M.; Wolf, E.; Hecht, E. Principles of Optics: Electromagnetic Theory of Propagation, Interference and Diffraction of Light. *Phys. Today* **2000**, *53*, 77–78. [CrossRef]
66. Pluta, M. Simplified polanret system for microscopy. *Appl. Opt.* **1989**, *28*, 1453. [CrossRef]
67. Thingujam, K.; Alapati, P.R.; Choudhury, B.; Bhattacharjee, A. Optical studies of a liquid crystalline compound 6O.6. *Liq. Cryst.* **2013**, *40*, 810–816. [CrossRef]
68. Ramakrishna, M.; Rao, N.; Prasad, P.V.D.; Pisipati, V.G.K.M. Orientational Order Parameter in Alkoxy Benzoic Acids—Optical Studies. *Mol. Cryst. Liq. Cryst.* **2010**, *528*, 49–63. [CrossRef]
69. Prasad, P.V.D.; Pisipati, V.G.K.M. Simple, Accurate and Low Cost Optical Techniques for the Measurement of 1. Birefringence in Liquid Crystals and 2. Variation of the Angle of the Small Angled Prism with Temperature. *Mol. Cryst. Liq. Cryst.* **2009**, *511*, 102–111. [CrossRef]
70. Manohar, R.; Shukla, J. Refractive indices, order parameter and principal polarizability of cholesteric liquid crystals and their homogeneous mixtures. *J. Phys. Chem. Solids* **2004**, *65*, 1643–1650. [CrossRef]
71. Vuks, M. *Electrical and Optical Properties of Molecules and Condensed Matter*; Leningrad Univ. Publ.: Leningrad, Russia, 1984.